abdus salam
international centre for theoretical physics

SMR: 1098/7

WORKSHOP ON THE STRUCTURE OF BIOLOGICAL MACROMOLECULES

(16 - 27 March 1998)

"EXAFS Spectroscopy: A Brief Introduction"

presented by:

Gilberto VLAIC
Sincrotrone Trieste
ELETTRA SCpA Experimental Division
Padriciano, 99
I-34012 Trieste
Italy

Workshop on The Structure of Biological Macromolecules

Trieste, 16 - 27 March 1998

EXAFS spectroscopy: a brief introduction

Gilberto Vlaic
Chemical Science Department, University of Trieste
and
ELETTRA SCpA Experimental Division

and

D. Andreatta, P. E. Colavita, E. Fonda
Chemical Science Department, University of Trieste

Part one

EXAFS: origin, theory and data processing

Introduction

The X-ray linear absorption coefficient of a certain atom, which is indicated as μx, is a monotone decreasing function of energy. It shows some discontinuities known as absorption edges (1). They occur when the energy of the incident photons is equal to the binding energy of a particular electron of the atom.

Picture 1 shows this behaviour for metallic Rh. It is possible to recognise four edges due to K and L electrons.

The edge energy is characteristic of each atom, so the absorption spectrum of a sample shows as many edges as the number of elements contained in it.

The absorption coefficient decreases monotonically versus energy, between two edges, only in the case of isolated atoms, for example in a monatomic gas. In any other situation the spectrum shows oscillations that extend from the edge for some hundreds eV. Picture 2 shows the absorption spectrum of the K edge of metallic Rh.

Origin of the EXAFS signal

When the incident photon has an energy greater than the edge energy, it is able to extract a core electron. The photoelectron emitted in this process has a kinetic energy equal to:

$$E=E_X-E_0 \qquad (1)$$

The photoelectron can be represented as a wave with wave vector modulus:

$$\left|\vec{k}\right| = \frac{2\pi}{\lambda} = \sqrt{\frac{8\pi^2 m}{h^2}\left(E_x - E_0\right)} = \sqrt{0.2624 \cdot E} \qquad (2)$$

In the case of an isolated atom, the photoelectron propagates as an non-perturbed isotropic wave (fig. 3a). In the presence of neighbours a scattering process can take place instead (fig. 3b). This leads to an interference phenomenon involving original and scattered waves that modify the interaction probability between the bonded electron and the incident photon. Constructive interference increases while destructive interference decreases the absorption coefficient of the emitting atom.

The EXAFS oscillation arises from this interference phenomenon. The total scattering amplitude depends on type and number of neighbours and so does the EXAFS oscillation amplitude. The type of interference, for a given energy of the photoelectron, depends on the distance between emitting and scattering atoms, so EXAFS signal contains information on interatomic distances too.

It is theoretically proved that the EXAFS signal given by only one type of scatterers at a single distance is a sinusoidal oscillation. In the presence of several atom types and/or distances the signal appears more complicated, anyway it is the sum of various sinusoidal functions. The EXAFS signal also contains information on thermal and structural disorder.

The EXAFS signal is usually defined as a function of wave vector **k** and it is mathematically defined as follows:

$$\chi(k) = \frac{\mu X - \mu_1 X}{\mu_1 X} = \frac{\mu X}{\mu_1 X} - 1 \qquad (3)$$

where μx is the experimental absorption coefficient and $\mu_1 x$ is the intrinsic atomic absorption coefficient. The aim of dividing by $\mu_1 x$ is the normalisation of the signal.

For core electrons, within the dipole approximation, the probability of X-ray absorption is given by:

$$P_{if} = \frac{2\pi^2 e^2}{m^2 \omega} |M_{if}|^2 \rho(E_f) \qquad (4)$$

where i and f stand for initial and final state of the electron, e and m are its charge and mass, $\rho(E_f)$ is the state density available to the electron (it is considered as a free electron so there is a continuos distribution of states), ω is the incident photon frequency and $|M_{if}|$ is a dipole matrix element related to the transition of the electron from i to f state.

$$|M_{if}| = \langle \Psi_f | \vec{p} \cdot \vec{e} | \Psi_i \rangle \qquad (5)$$

where p is momentum operator, e is the electric field vector of the X photon, ψ_f and ψ_i are wave functions for i and f states.

ψ_f depends on the absorbed photon energy and can be written as a linear combination of two terms: the wave function for the photoelectron outgoing the excited atom and a perturbing term ψ_{sc} which takes into account backscattering.

The absorption coefficient is proportional to the absorption probability, so:

$$\chi(k) = \frac{\langle \Psi_{out} + \Psi_{sc} | \vec{p} \cdot \vec{e} | \Psi_i \rangle}{\langle \Psi_{out} | \vec{p} \cdot \vec{e} | \Psi_i \rangle} - 1 \qquad (6)$$

In 1974 E. A. Stern (2) suggested the following mathematical expression for the EXAFS signal:

$$\chi(k) = \frac{1}{k} \sum_i \frac{N_i}{R_i^2} \cdot \exp(-2\sigma_i^2 k^2) \cdot \exp\left(\frac{-2R_i}{\lambda(k)}\right) \cdot |f_i(k)| \cdot \sin[2kR_i + \Phi_i(k)] \qquad (7)$$

where:

- k is the wave vector modulus for the photoelectron
- N_i is the number of atoms of type i at distance R_i from the absorber
- the exponential term $\exp(-2\sigma_i^2 k^2)$ takes into account fluctuations of interatomic distances due to structural and/or thermal disorder
- the exponential term $\exp\left(\frac{-2R_i}{\lambda(k)}\right)$ takes into account finite elastic mean free paths of photoelectrons $\lambda(k)$(between 5 and 10 Å for photoelectron energies from 30 to 1000 eV)
- $|f_i(k)|$ is a scattering amplitude function characteristic of the i-th atom
- $\Phi_i(k)$ is a phase function which accounts for the varying potential field along which the photoelectron moves, it can be expressed as the sum of two potential terms

$$\Phi_i(k) = 2\delta(k) + \varphi_i(k)$$

the former given by the absorber, the latter given by the scatterer

The EXAFS signal is a sum of sinusoidal functions whose amplitudes depend on the number and type of atoms at distance R and whose frequencies depend on interatomic distances and phase functions.

Equation (7) is valid in the case of non-oriented samples (crystalline powders, solutions and gases) and also for monocrystals, whenever a common X-ray tube is used . Using synchrotron light sources with monocrystals implies a correction of equation (7): it must be multiplied by $3\cos^2\Theta$, where Θ is the angle between the absorber-scatterer axis and the synchrotron orbital plane. This term takes into account the polarisation of synchrotron light (electric field vector lies on the orbital plane).

This formula is based on two hypotheses:
- only single backscattering processes occur, excluding multiple scattering processes, which are important only for low k values (when the mean free path of the electron is long, about 10-100Å for energies between 0 to 20 eV) and for collinear or nearly collinear systems at every energy;
- thermal or static disorder is moderate and distance distributions can be described with gaussian distributions.

In this way it is possible, knowing phase and amplitude functions, to obtain structural information on the sample by the EXAFS signal analysis.

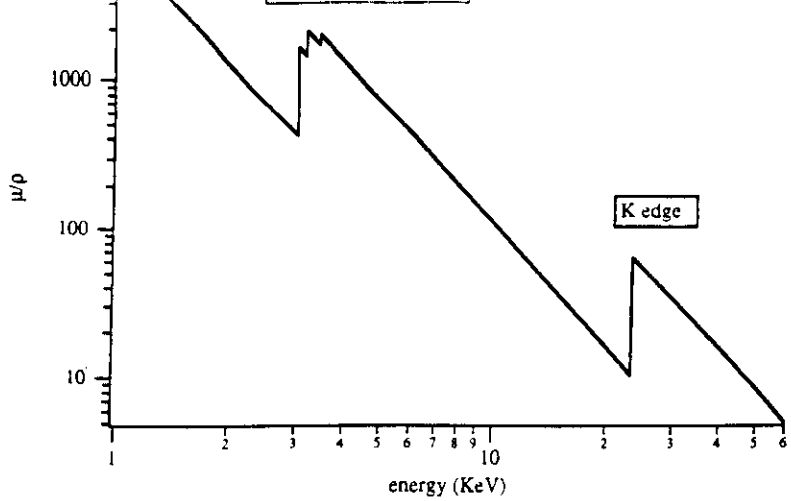

Fig. 1

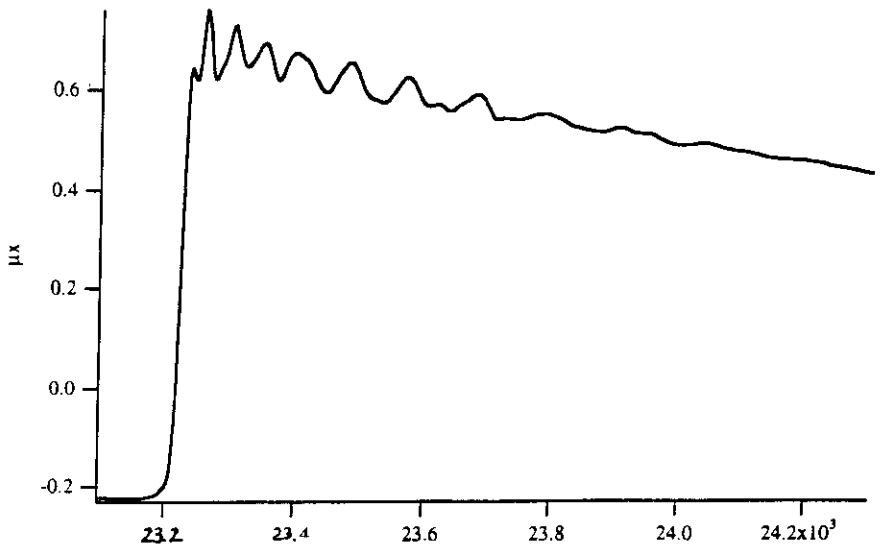

Fig. 2

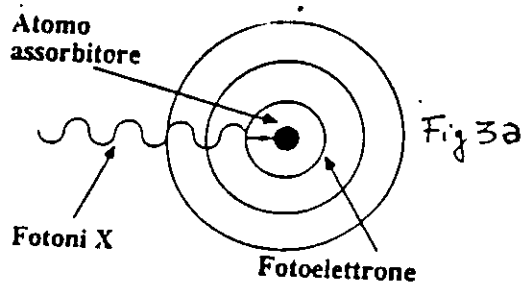

Fig 3a

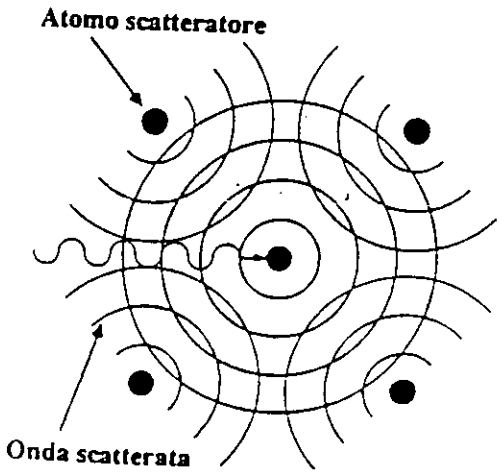

Fig 3b

Experimental methods

The most common EXAFS beam-line works in transmission. It collects data measuring how beam intensity decreases as it passes through the sample while scanning energy.

As in any spectroscopy a light source is needed. EXAFS spectroscopy requires a polychromatic X-ray source as an X-ray tube or a synchrotron. The former was the first source used for spectra recording but it gives a low quality signal that takes long recording time because of bremsstrahlung low intensity. Due to this, EXAFS spectroscopy remained only a scientific curiosity until the utilisation of synchrotron light. Nowadays EXAFS laboratory spectrophotometers also exist. They work using rotating anode tubes as light sources and they are able to record spectra in a couple of hours. Anyway these instruments give low quality signals despite their high costs. For a historical and technical review see references (3, 4, 5, 6, 7).

Hence, the best light sources for EXAFS spectroscopy remain synchrotrons. Picture 4 shows EXAFS-I beam-line at LURE laboratory (Paris, France) which works in transmission.

In position 1 there is a shutter (named OBX-S) which stops the beam to allow any operation on the line. It is possible to open the shutter only when all security systems are working.

In position 2 there is a Be window 100 μm thick. It isolates the ultra-vacuum inside the ring from the laboratory environment. This window is almost transparent to high energy photons, hence it is possible to measure K edge spectra from P to Sn and L edge spectra from Y to Pu (1). The ring characteristics determine this upper limit.

In position 3 and 4 there are slits for limiting width and height of the beam. Usually it has a 2x5 mm dimension.

In position 5 there is a "channel-cut" monochromator that allows to obtain photons with fixed energies or to make an energy scanning. It works following Bragg's law:

$$2d_{hkl}\sin(\Theta) = n\lambda \quad (8)$$

where Θ varies from 10° to 56°.

The following equation relates photon energy in eV to wavelength in Å:

$$E_x = \frac{12398.52}{\lambda} \quad (9)$$

In position 6,8 and 7 there are features that allow to measure I_0 (incident intensity) and I (final intensity), and a sample holder respectively. 6 and 8 are usually ionisation chambers.

Experimental spectra are recorded scanning energy from about 100 eV below the edge to 1000 eV above it. Energy steps are of 2 or 3 eV and each point takes 1 or 2 seconds. Therefore a whole spectrum takes from 10 to 30 minutes.

As it is well known, Lambert-Beer law relates intensities I_0 and I to the absorption coefficient:

$$\ln\frac{I_0}{I} = \mu x \quad (10)$$

Because of the angular rotation of the crystals inside the monochromator, the beam can shift up or down. Light must pass through the sample always at the same position, so either the sample follows the beam by placing it on a micrometric table, or it is necessary to change the monochromator mechanism to obtain a fixed beam.

Data processing

Nowadays there is no standard method for data analysis, but there is an International Committee that is trying to establish standard procedures. Until now it has given some recommendations contained in two reports (8, 9). Owed to this and to the large number of particular cases, a long training period is needed to obtain correct information.

Programs used for carrying out data analysis in the following examples were written by Alain Michalowicz taking into account the recommendations mentioned above (10).

The first step in data analysis is signal extraction by background removing . This delicate operation can be divided into three steps:

a) choosing a threshold energy, for defining the wave vector;

b) pre-edge extrapolation (named $\mu_0 x$)

c) atomic absorption modelling (named $\mu_1 x$)

After these steps it is possible to obtain the EXAFS signal as:

$$\chi(E) = \frac{\mu x(E) - \mu_1 x(E)}{\mu_1 x(E) - \mu_0 x(E)} \qquad (11)$$

Lengerer and Einsenberger (11) suggested a method that is widely used. Atomic absorption modelling is carried out using polynomial curves or cubic splines and $\mu_1 x - \mu_0 x$ is evaluated using Heitler's formula (12). The edge-jump, which is the only unknown parameter, is calculated with a pre-edge extrapolation.

Picture 5 shows the complete signal extraction procedure for IrO_2.

The raw EXAFS signal obtained with the above procedure is built of many sinusoidal waves. Fourier Transform (FT) is the standard tool used for frequency separation. This operation transforms each sinusoidal component in an FT modulus peak, going from k($Å^{-1}$) space to R(Å) space. The outcoming function is a radial distribution.

Two problems related to FT exist. The former is that $\chi(k)$ is highly damped so little information is contained at high k values. To minimise this problem $\chi(k)$ is multiplied by k^n before Fourier transforming, usually n is equal to 1, 2 or 3. The latter is that the signal has a limited number of points, therefore the Fourier integral is truncated. To minimise distortions and to avoid the presence of ripples in the FT modulus $\chi(k)$ is multiplied by a window W(k). Hence, the FT looks like:

$$F.T.(R) = \sqrt{\frac{1}{2\pi}} \int_{k_{min}}^{k_{max}} W(k)\, k^n\, \chi(k)\, \exp(2ikR)\, dk \qquad (12)$$

The height of the peaks depends on amplitude parameters contained in equation (7), while their position depends on phase parameters. Total or partial overlapping of more peaks often occurs.

If phase functions did not depend on k, maxima of the FT would fall at the correct interatomic distances. Since $\Phi(k)$ depends on k, peaks are shifted to lower R values (9).

Picture 6 shows the FT modulus for IrO_2. Peaks corresponding to Ir-Ir and Ir-O distances are clearly visible.

If $\chi(k)$ were badly extracted, some peaks would appear at too low R values to be physically significant . Peaks at low R mean that the signal contains low frequency components due to residues of atomic absorption. In this case it is better to repeat the signal extraction procedure.

Once different R values have been separated an inverse Fourier Transform is carried out, going from R(Å) space to k($Å^{-1}$) space, but only on limited intervals in R space. Each peak is individually transformed:

$$\chi_i(k) = \frac{\sqrt{2\pi}}{W(k)\ k^n}\int_{R_1}^{R_2} F.T.(R)\ \exp(-2ikR)\ dR \qquad (13)$$

The outcome of this operation is a $\chi_i(k)$ function related to absorber-scatterer pairs whose interatomic distances belong to that specific integration interval. Picture 7 shows the inverse FT (FT^{-1}) of the first peak in picture 6, which corresponds to an Ir-O pair.

Structural parameters can be obtained from $\chi_i(k)$ by means of a fitting procedure using known phase and amplitude functions. EXAFS analysis allows to obtain the number of neighbours, interatomic distances and an estimate of disorder around the central atom.

Phase and scattering amplitude functions are either theoretical or experimental functions.

Teo and Lee calculated theoretical functions in 1977 assuming that the photoelectron wave is a plane one (13, 14, 15). Better phases and amplitudes were obtained by McKale et al. in 1988 (17) without the plane wave approximation. In this case functions change with interatomic distances so they are calculated mathematically only for two distances while for other R values it is necessary to perform an extrapolation.

Experimental functions are extracted from proper reference samples whose structure is already known. These can be used thanks to the phase and amplitude transferability principle (16) that states as follows:

phases and amplitudes are insensitive enough to chemical environment in order to be extracted from a well-known sample and transferred to an unknown sample containing the same absorber-scatterer pair at a similar distance.

Phase functions can be extracted filtering FT peaks and using the following formula:

$$\Phi(k) = \arctg\frac{Re}{Im} - 2kR \qquad (14)$$

The amplitude can be obtained by:

$$A(k) = \exp(-2\sigma^2k^2)\ \exp\left(\frac{-2R}{\lambda(k)}\right)\ |f(k)| = \sqrt{Re^2 + Im^2}\ \frac{R^2}{N} \qquad (15)$$

These amplitude functions include the analyser's estimate of σ and $\lambda(k)$ for the reference sample, so final fit values for these parameters will be relative to the initial choice.

The k-scale is not an absolute one, because it depends on the choice of E_0 that is entrusted to the analyser's skills. Besides, threshold energy is slightly sensitive to chemical environment and sometimes monochromator fails too, adding other errors. Therefore it is necessary to redefine the k-scale introducing a ΔE_0 dependence:

$$k' = \sqrt{k^2 + 0.2624\ \Delta E_0} \qquad (16)$$

This operation aims at bringing phase and amplitude to the same scale of the signal, making the fit possible. This is true also using theoretical functions. Even though they are built on an absolute scale it is better to bring them to the experimental one.

Experimental phase and amplitude functions are better than theoretical ones because they do not contain calculus approximations. Anyway analysers must be careful to extract them using the same procedure as with the unknown sample (same integration limits and same windows) in order to introduce exactly the same truncation distortions.

Experimental functions are not always available because no proper reference compounds exist or because it is impossible to extract them. For instance metallic Fe does not allow to extract phase and amplitude for the Fe-Fe pair because Fe is surrounded by 8 atoms at 2.48 Å and 6 atoms at 2.86 Å and these two peaks overlap in the FT modulus.

In these cases the analyser is compelled to use theoretical functions. In order to obtain coordination numbers N_i it is necessary to estimate $\lambda(k)$. One of used functions, proposed by Lee and Beni (9), is:

$$\lambda(k) = \frac{1}{\Gamma}\left[\left(\frac{\eta}{k}\right)^4 + k\right] \qquad (17)$$

where Γ and η are numerical coefficients. η is equal to zero unless minimisation has to be carried over regions with $k<3$. Γ has to be determined by fitting procedures using a known model.

This technique allows to estimate structural parameters with a precision highly dependent on data and analysis quality. Usually errors are of about 0.01-0.02 Å for interatomic distances, and 5-15% for coordination numbers.

References

1) W. H. McMaster, N. Kerr del Grande, J. H. Mallet, J. H. Hubbel, Compilation of X-ray cross sections, UCRL-50174 sec. II rev. I (1969)
2) E. A. Stern, Phys. Rev. B, 10, 3027 (1974)
3) R. de L. Kronig, Zeit. Phys., 70, 317 (1931)
4) R. de L. Kronig, Zeit. Phys., 75, 191 (1932); ibidem, 468
5) H. Petersen, Zeit. Phys., 80, 258 (1933)
6) G. Vlaic, S. Enzo, Rend. Sem. Fac. Sci. Univ. Cagliari, 49, 399 (1979)
7) S. Steeb, P. Lamparter, The Rigaku Journal, 3, 13 (1986)
8) Report of the International Workshop on Standards and Criteria in X-Ray Absorption Spectroscopy, Physica B, 158, 701 (1989)
9) Report of the International Workshop on Standards and Criteria in X-Ray Absorption Spectroscopy, in "X-Ray Absorption Fine Structure" (ed. S. S. Hasnain) Hellis Horwood, Chicester (1991), pag. 751
10) A. Michalowicz, in "Logiciels pour la Chimie" (ed. Societé Française de Chimie), Paris, 1991, pag. 751
11) B. Lengerer and P. Eisenberger, Phys. Rev. B, 21, 4507 (1980)
12) W. Heitler, in "Quantum Theory of Radiation", third edition, Oxford University Press
13) B. K. Teo, P. A. Lee, A. L. Simmons, P. Eisenberger and B. M. Kincaid, J. Am. Chem. Soc., 99, 3854 (1977)
14) P. A. Lee, B. K. Teo, A. L. Simmons, J. Am. Chem. Soc., 99, 3856 (1977)
15) A. G. McKale, B. W. Veal, A. P. Paulikas, S. K. Chan and G. S. Knapp, J. Am. Chem. Soc., 110, 3763 (1988)
16) P. H. Citrin, P. Eisenberger and B. M. Kincaid, Phys. Rev. Lett., 36, 1346 (1976)
17) P. A. Lee and G. Beni, Phys. Rev. B, 15, 2862 (1977)

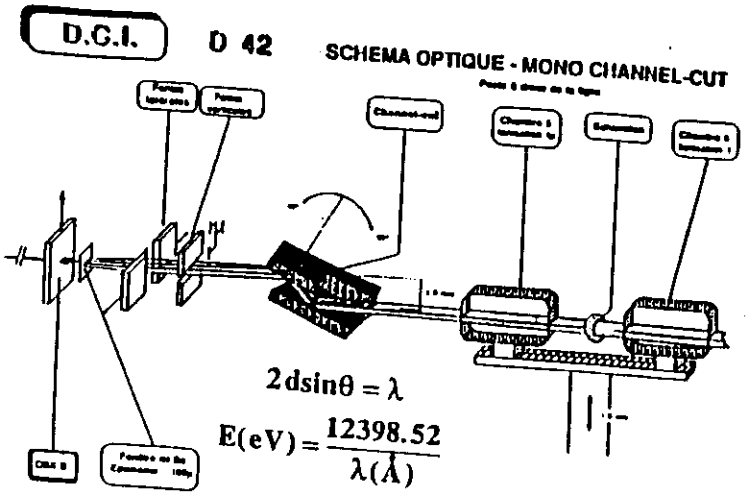

Fig. 4

Calcolo Trasformata di Fourier
(da spazio **k** in Å-1 a spazio **R** in Å)

$$F.T.(R) = \sqrt{\frac{1}{2\pi}} * \int_{k_{min}}^{k_{max}} W(k) * k^n * \chi(k) * \exp(2ikR) * dk$$

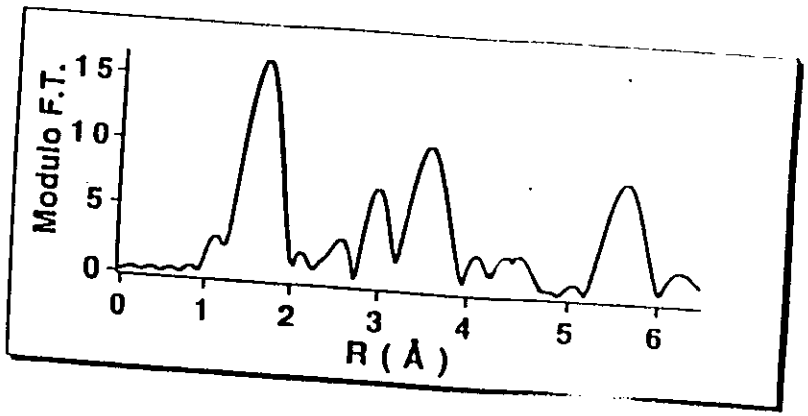

Fig. 6

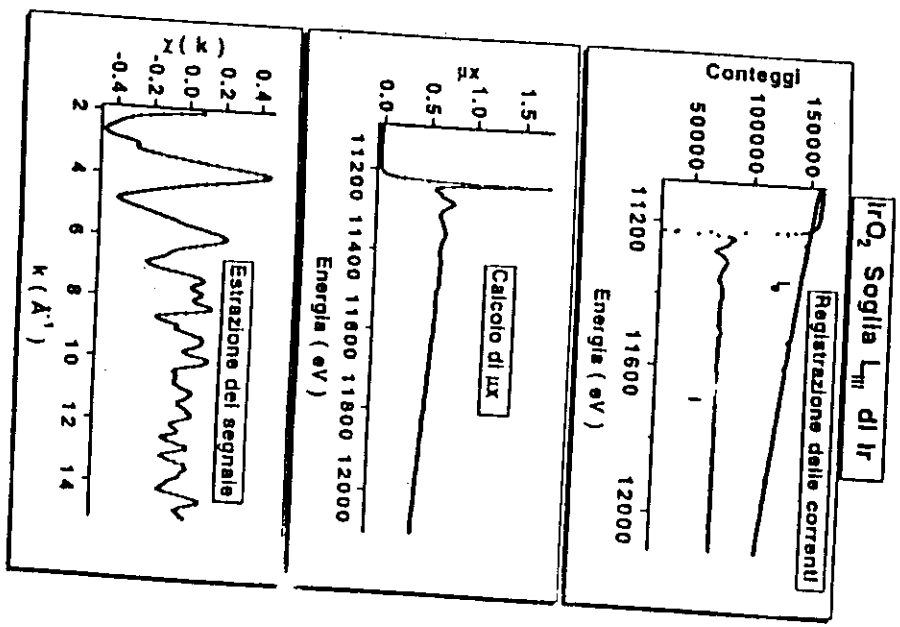

Fig. 5

Filtrazione da spazio R (Å) a spazio k (Å-1) di parte di F.T.: contributo parziale dell'intero segnale EXAFS

$$\chi_i(k) = \frac{\sqrt{2\pi}}{k^n W(k)} * \int_{R_1}^{R_2} F.T.(R) * \exp(2ikR) * dR$$

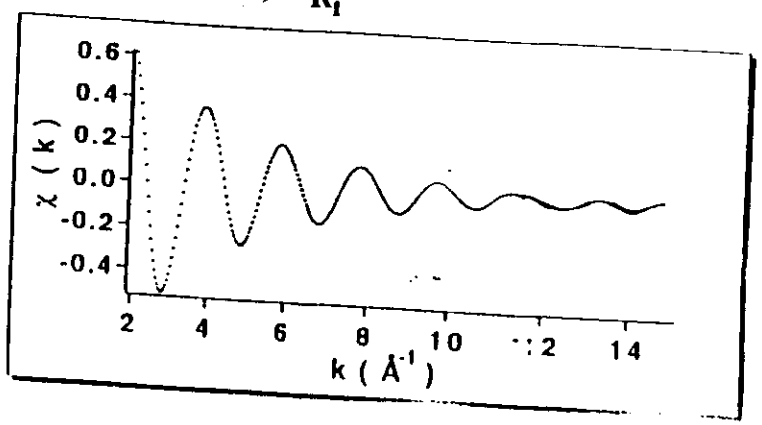

Fig. 7

Part two

Data analysis: statistics & error determination

Introduction

Is EXAFS spectroscopy a promising new technique?
H. Bertagnolli and T. S. Ertel gave an answer to this question in one of their last papers:

«... On first glance, the answer is yes. The element-specific determination of local structures is possible, independent of the samples physical state and even at very high dilution. The action of catalysts can be investigated and reactions can be studied in-situ. On second glance, the answer is no. Experiments must rely on synchrotron radiation, as the laboratory EXAFS methods are not yet far enough developed. This necessitates long-term planning of experiments, short beam times and dependence on the research policy of the operator. The analysis of spectra is difficult; interpretation is only possible with the help of extensive spectral simulations, which is in contrast to many common spectroscopic techniques. Compared to these efforts, the information obtained is minimal.

Neither of these viewpoints does justice to EXAFS spectroscopy. Its utilisation is only sensible when detailed information about the immediate short-range order around a specific atom type is necessary, and when this information is not accessible by other techniques. Even then it is wrong to expect too much of EXAFS spectroscopy. If the short range order is characterised by a broad distance distribution, or if different backscatterers are present at similar distances, EXAFS spectroscopy cannot yield unambiguous results. As long as these limitations are kept in mind, and systems to be studied are selected accordingly, EXAFS spectroscopy, in combination with other techniques, can supply new observations, maybe even key information.» (1)

The International Workshop on Standard Criteria in XAS published two reports containing other important observations:

«The major weakness in many EXAFS publications is the assessment of errors associated with deduced parameters.» (2)

«The field of XAFS spectroscopy has grown dramatically over the last two decades and has significantly matured. Improvements in experimental methods, as well as refinements to the theory and data analysis, have great improved the range of reliability of the technique. In spite of these successes, however, the average technical quality of papers based on XAFS remains disappointingly low...(and) has harmed the credibility of the XAFS literature as a whole.» (3)

Keeping in mind these limitations and recommendations, EXAFS spectroscopy remains, however, a powerful research tool and it is massively used in catalysis. Since no restrictions exist on the physical state of the sample or on its environment, it is possible to accomplish measurements during thermal and/or gaseous catalytic treatments. Therefore EXAFS is able to follow catalysts along their usual steps: as prepared, after desiccation, activation, reaction, poisoning and regeneration.

A spectrum recording takes from 15 minutes up to three hours, so kinetic studies are impossible to perform and only in-equilibrium systems can be analysed. However there are two other EXAFS techniques which take shorter recording times. The former is known as "Quick-EXAFS" and requires only a couple of minutes. The latter is dispersive EXAFS and takes a couple of seconds.

Data analysis and statistics

As in any other technique, outcoming values must have their error bars; particularly in EXAFS, where the analysis is based on fitting procedures, the statistical analysis becomes a very important tool.

The minimisation procedure is carried out over the following function:

$$F(P_i) = A = \sum_k w(k)\left[\chi_{exp}(k) - \chi_{th}(k, P_i)\right]^2$$

where P_i are the fitting parameters and w(k) is a weighting function.

A residual factor can be defined also as:

$$\rho = \frac{A}{\sum_k w(k)\chi^2_{exp}(k)}$$

Another important quantity is the number of independent points N_{ind}, which is strictly related to the maximum number of fittable parameters given by:

$$N_{par} = N_{ind} - 1$$

Since the EXAFS signal undergoes two Fourier integrations, the number of independent points is given by the following formula:

$$N_{ind} = \frac{2 \cdot \Delta k \cdot \Delta R}{\pi} + 2$$

where Δk is the fitting interval (NOT the Fourier integration interval) and ΔR is the filtering interval. The term "+2" is due to the discrete nature of data.

The number of degrees of freedom is given by:

$$\nu = N_{ind} - N_{par}$$

Systematic errors in EXAFS measurements can arise from any element on the beam-line. Particularly, the presence of harmonics and inhomogeneities in the sample may reduce signal amplitude and hence lead to deceiving neighbour numbers. Detectors are also error sources, for instance if detectors are ionisation chambers the chosen gas is an important factor. An uncontrollable error can derive from the beam itself.

Nowadays there are no standard methods for error determination in EXAFS spectroscopy from experimental errors yet. The following treatment is the one used by our team. It takes care of the recommendations of the Standardisation Committee (2,3), using methods which yield (probably) overestimated errors.

All statistical concepts are based on repeating each single measure 3 times or more, in order to define an average with its standard deviation. Hence recording each spectrum n times, that is recording every point n times, the average is given by:

$$\overline{k_i\chi(k_i)} = \frac{\sum_{j=1}^{n} k_i\chi_j(k_i)}{n}$$

and standard deviation by:

$$s(k_i) = \sqrt{\frac{\sum_{j=1}^{n}\left[\overline{k_i\chi(k_i)} - k_i\chi_j(k_i)\right]^2}{n-1}}$$

For fitting procedures it is necessary to define a function strictly related to the "goodness of fit", hence a function which "says" how far the fitting curve is from experimental data. One of the most used ones is CHI-SQUARED:

$$X^2 = \sum_i \frac{1}{s_i^2}\left[y_i - y(x_i)\right]^2$$

where y_i are experimental data and y(x) is the chosen function. In the case of EXAFS it becomes:

$$X^2 = \sum_i \left[\frac{k_i\chi_{exp}(k_i) - k_i\chi_{th}(k_i)}{s^2(k_i)}\right]^2$$

Another useful quantity is the REDUCED CHI-SQUARED defined as follows:

$$X_\nu^2 = \frac{X^2}{\nu}$$

For a good fit X_ν^2 tends to one. Fits with X_ν^2 lower than one are equally significant to those with X_ν^2=1.

Once chi-squared has come to a minimum, error determination becomes possible varying each parameter separately while refining the others until X^2 changes of n units, accordingly to the chosen confidence interval. In the case of a confidence interval of 68%, n is equal to 1. Other values of n are tabulated in proper handbooks.

When a fit has reached a minimum using a certain structural model, a new fit can be performed adding more parameters. A question arises: does the improvement in fit quality justifies a higher number of parameters?

As more parameters are added, fitting function complexity increases while X^2 decreases. However, X_ν^2 behaviour depends on the number of degrees of freedom, which decreases while increasing the number of parameters. One of the most used comparison criteria between two fits is the F-Test (6, 7). It gives a hint on choosing the best fit by comparing their X_ν^2 ratio to those tabulated on Fisher's tables.

More information on statistics can be found on the books written by Taylor (4) and Bevington (5).

References

1) H. Bertagnolli and T. S. Ertel, Angew. Chem. Int. Ed. Engl., 33, 45 (1994)
2) F. W. Lytle, D. E. Sayers and E.. A. Stern, Phisica B, 158, 701 (1989)
3) Report on the International Workshop on Standard and Criteria in XAFS, in "X-Ray Absorption Fine Structure" (ed. S. S. Hasnain) Ellis Horwood Publishers, (1991) pag. 751
4) J. R. Taylor, An Introduction to Error Analysis, Oxford University Press (1982)

5) P. R. Bevington and D. K. Robinson, Data Reduction and Error Analysis for the Physical Sciences, McGraw-Hill (1992)
6) R. W. Joyner, K. J. Martin and P. Meehan, J. Phys. C Solid State Phys., 20, 4005 (1987)
7) J. Freund, Phys. Lett. A, 157, 256 (1991)

Part three

Examples

Introduction

EXAFS spectroscopy is an important technique in various fields of natural science, from physics to biochemistry. Since in catalysis samples show highly disordered structures, EXAFS is one of the few tools for structural investigation. In this section two applications of EXAFS in catalysis are illustrated. The first is a study on a Pt zeolite system and the second is a three way catalyst used for car silencers.

Pt/KL zeolite catalyst under oxidation, reduction and reaction cycles

This work was performed by M. Bellatreccia et al. and C. Dossi et al. (1, 2)

This Pt/KL zeolite is a reforming catalyst very active and selective in conversion of methylcyclopentane (MCP) to benzene. It was prepared via CVD (Chemical Vapour Deposition) at 70°C using platinum hexafluoroacetylacetonate under flowing argon. The amount of Pt deposited was about 1% in weight.

Exploiting EXAFS capability of in-situ analysis, spectra were recorded after the following steps:

A) 1- After deposition
2- After reduction under H_2
3- After calcination under O_2
4- After second reduction under H_2

B) 1- After reduction
2- After catalytic test with MCP

A)

Pictures a, b and c show the EXAFS signal, the FFT and the first peak filter respectively of the sample after deposition. Data analysis shows that there is no Pt-Pt interaction and that the precursor structure is maintained. This stands for a low interaction between the zeolite cage and Pt-O4 groups.

Pictures d, e and f refer to the sample after first reduction. During this step, reduction eliminates ligands and leads to the formation of metallic particles. This procedure avoids the initial calcination which leads to the formation of Pt oxide particles. Assuming a close-packed structure, the estimate diameter of the cluster does not exceed 7 Å. The cluster is well confined in the zeolite cavity whose dimensions are 5Å x 13Å x 11Å. No Pt-O interaction can be seen at this stage. This could have two explanations:

- Pt-O interaction is negligible compared to Pt-Pt interactions

AND/OR

- Pt-O coordination distances cover a wide range, producing a flat distribution on the FFT of the experimental spectrum.

The large amount of noise contained in data prevents from extracting the cluster form.

Pictures g, h and i refer to the sample after calcination. Data analysis reveals the presence of metal particles not completely oxidised to PtO_2, located inside the zeolite cavities.

Pictures l, m and n refer to the sample after the second reduction. The fit results closely match those obtained after the first reduction. This suggests that the cluster structure remains

unchanged after thermal and chemical treatments and no sintering takes place. This conclusion was also confirmed by the fact that its catalytic performances were retained even after two oxidation cycles (not shown here).

B)

Pictures d, e and f refer to the sample after reduction. They show the same structure of the reduced sample described above.

Pictures g, h and i refer to the sample after a catalytic test with MCP. Data analysis shows no evidence of a Pt-C contribution to the signal. This confirms the absence of a significant carbon deposition on the metal surface. The reactivity of the system remains unchanged after a 24 hours work. If it had been coked the catalyst would have been deactivated.

References:

1) M. Bellatreccia et al., J. Chem. Soc. Faraday Trans, 91, 2045 (1995)
2) C. Dossi et al., J. Catal., 145, 377 (1994)

NO decomposition and CO oxidation catalysts (three way catalysts)

A very efficient catalytic system for NO decomposition and CO oxidation is built by using a solid solution of two oxides as a support for noble metals. This solution contains specifically CeO_2 and ZrO_2, while the noble metal is Rh, Pt or Pd.

Pure ZrO_2 is monoclinic. Zr has seven oxygen neighbours at seven different distances (1). Pure Ceria has a fluorite structure. Ce has 8 oxygen neighbours at 2.34 Å. When an oxide like CeO_2 is added to ZrO_2 the structure becomes tetragonal or cubic (2). Nevertheless, in powder diffraction spectra there are some peaks which cannot belong to these structures.

There are three hypothetical structures for cubic-stabilised Zirconia:

- 8 Oxygen atoms at 2.20 Å
- 4 Oxygen atoms at 2.07 Å and 4 at 2.35 Å
- 6 Oxygen atoms at 2.14 Å and 2 at 2.42 Å

Spectra of the following samples were studied:

Rh (5% in weight) on:
Zr 80% Ce 20% (T)
Zr 40% Ce 60% (C)
Zr 20% Ce 80% (C)
Zr 50% Ce 50% (C)
Zr 50% Ce 50% (T)

where T stands for tetragonal, C for cubic, and the percentages are molar ratios. Each spectrum was recorded at Zr and Rh K edges, and at L_{III} edge of Ce, as prepared, after reduction and after catalytic cycles with NO, CO and NO+CO.

Data analysis in this case aims at determining whether the two oxides form a solid solution or stay separated and, if the first hypothesis were confirmed, at solving the sample structure.

Pictures a, b, c and d show the EXAFS signal, its FFT and the first and second peak filters respectively for Zr 50% Ce 50% (C) at Zr edge. The first filter contains, at first sight, a contribution of light atoms to the signal, while the second one shows a more complex structure owed to metallic second neighbours.

Picture e shows how FFT modulus changes as the molar ratio changes. While the first peak shows little variation (except for the first sample), the second peak remarkably varies in

height from one sample to another. The decreasing magnitude of the Zr-cation peak has always been explained as owed to an increasing static disorder of the system (3).

Actually peak heights decrease because Zr-Zr and Zr-Ce phases oppose to each other, as picture f shows (the dotted curve has been shifted of π in this graph). Picture g and h show three theoretical signals given by 12 Zr, 12 Ce and 6 Zr+6 Ce at 3.70 Å and their FFTs: it is clearly proved that the oscillation amplitude and peak heights decrease when simulating a composed signal.

The question on whether the oxides form a solid solution or stay basically separated constituting microphases is still open. Pictures j and k show two fits carried out for $k > 6$ Å^{-1}, in order to make negligible the presence of oxygen atoms. The first one was performed assuming that the oxides stay separated, hence considering each Zr surrounded by 12 Zr neighbours. The second one simulates a solid solution in which each Zr is surrounded by 12 Zr and Ce neighbours with coordination numbers according to their molar ratios. The hypothesis of a solid solution is obviously confirmed.

Picture l shows the fit carried out over the entire k-space interval, including oxygen atoms in the theoretical spectrum.

Fitting the first peak filter was a hard task. None of the structures suggested in literature for cubic-stabilised Zirconia worked out as expected (pictures m and n) so various sets of coordination numbers and distances were tested (more than 40!). Theoretical functions containing from one to three different interatomic distances and total coordination numbers between 6 and 8 atoms were examined (some examples are illustrated in pictures o and p). At the end more than a single reasonable fit was obtained, therefore only a statistical analysis, carried out with the F test, allowed to settle which one was the best (picture o).

The fit that survived to this statistical comb can be explained keeping in mind the ideal fluorite structure in picture q. Fit results would suggest that two oxygen atoms around each Zr go further away and approach another Zr atom while keeping Ce-O distances unchanged. This hypothesis is also confirmed by data analysis of spectra taken at Ce edge, and by other analytical techniques.

References:

1) D. K. Smith and H. W. Newkirk, Acta Cryst., 18, 983 (1965)
2) C. J. Howard, R. J. Hill and B. E. Reichert, Acta Cryst., B44, 116 (1988)
3) P. Li, I. W. Chen and J. E. Penner-Hahn, J. Am. Ceram. Soc., 77, 1281 (1994)

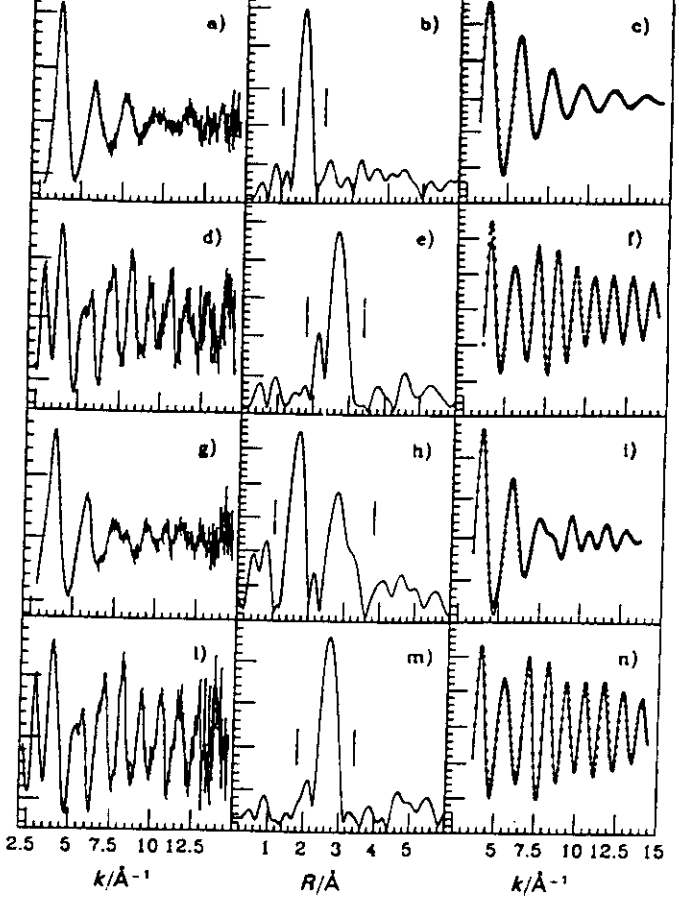

sample	shell	N	R/Å	$\sigma^2/10^{-2}$ Å^2
I	Pt–O	4.0 ± 0.4	1.98 ± 0.02	5.6 ± 0.5
II	Pt–Pt	5.5 ± 0.5	2.76 ± 0.02	7.3 ± 0.7
III	Pt–O	2.5 ± 0.2	2.02 ± 0.02	7.3 ± 0.7
	Pt–Pt	1.0 ± 0.2	2.76 ± 0.02	6.4 ± 0.6
	Pt–Pt	1.0 ± 0.2	3.07 ± 0.02	7.1 ± 0.7
IV	Pt–Pt	6.0 ± 0.5	2.76 ± 0.02	7.4 ± 0.7

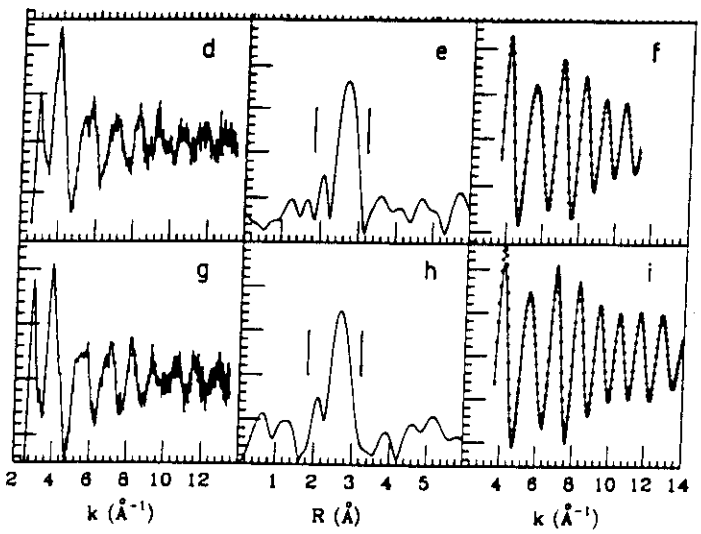

After reduction

After catalytic test with MCP

Shell

Pt - Pt

N

6.1 ± 0.5

R

2.76 ± 0.02

σ^2

7.5 ± 0.7

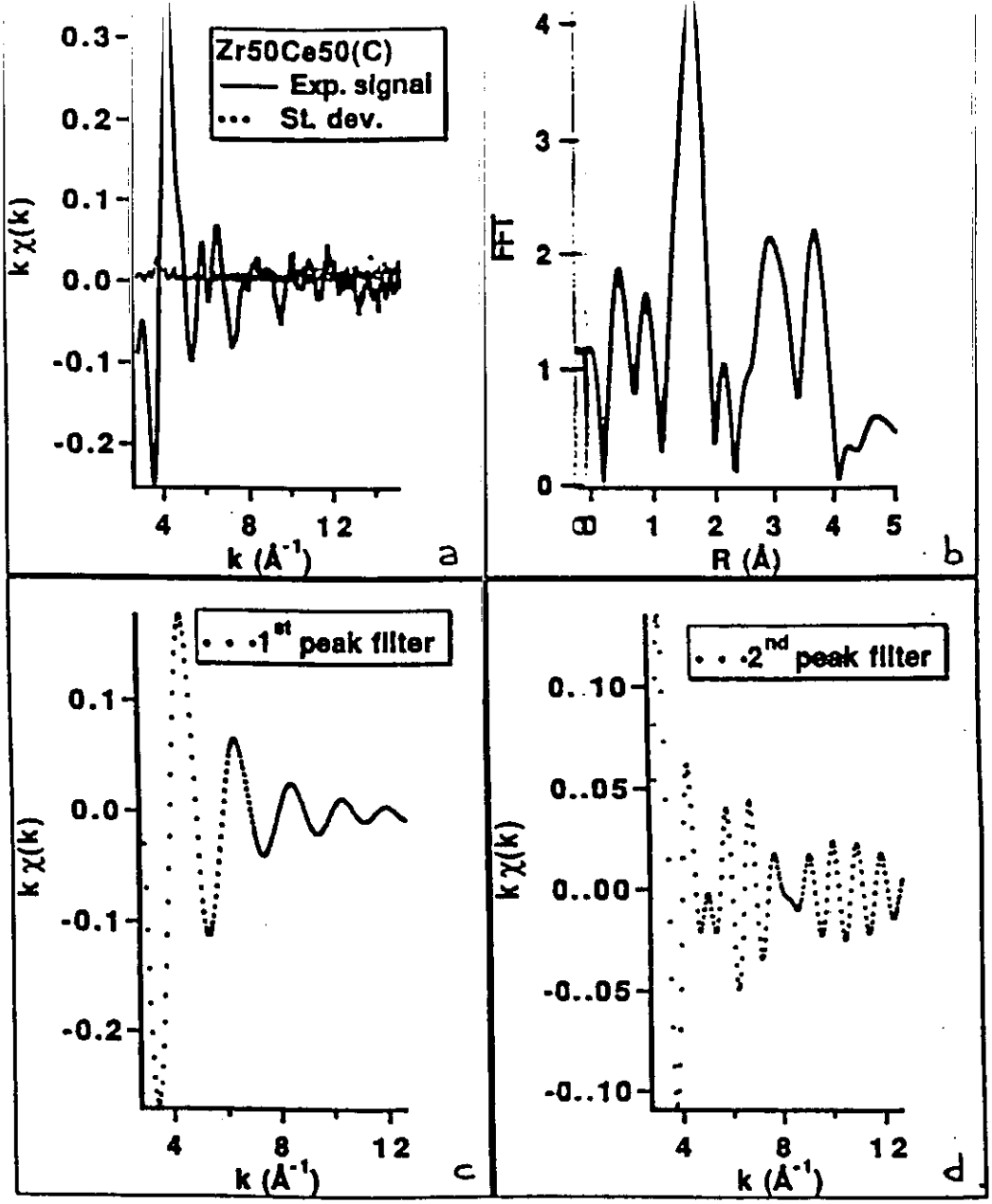
Zr50Ce50(C)
Exp. signal
St. dev.
k χ(k)
k (Å⁻¹)
a
FFT
R (Å)
b
1st peak filter
c
2nd peak filter
d

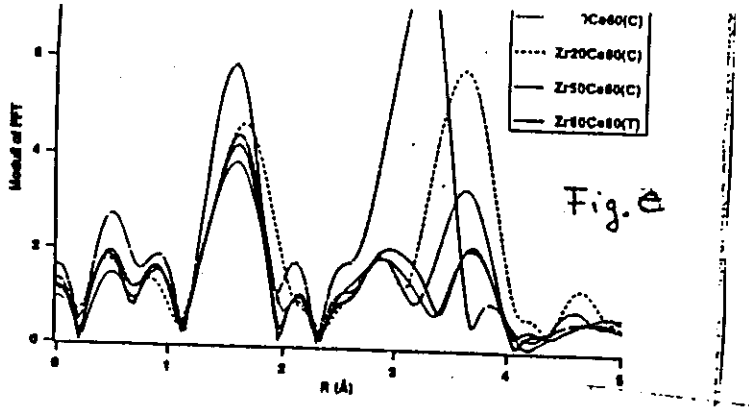

Fig. e

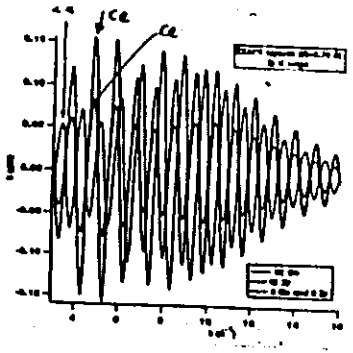

Fig. g

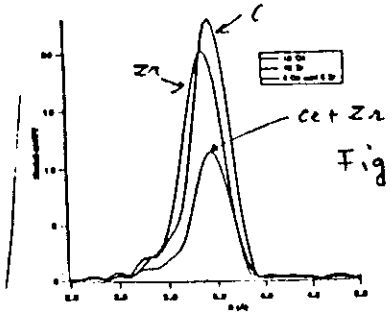

Fig. h

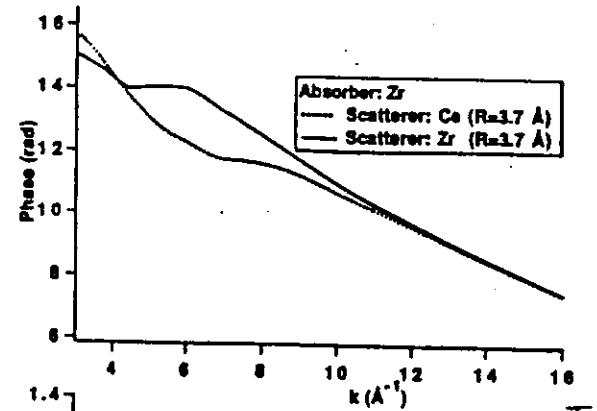

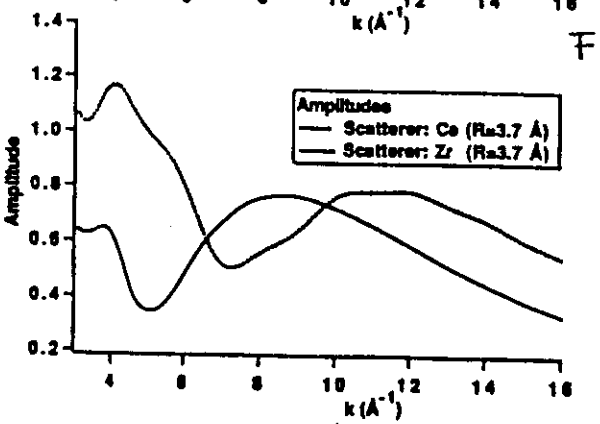

Fig. f

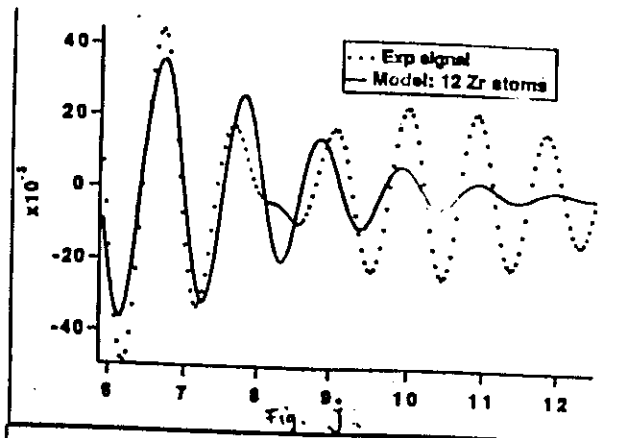

Fig. j

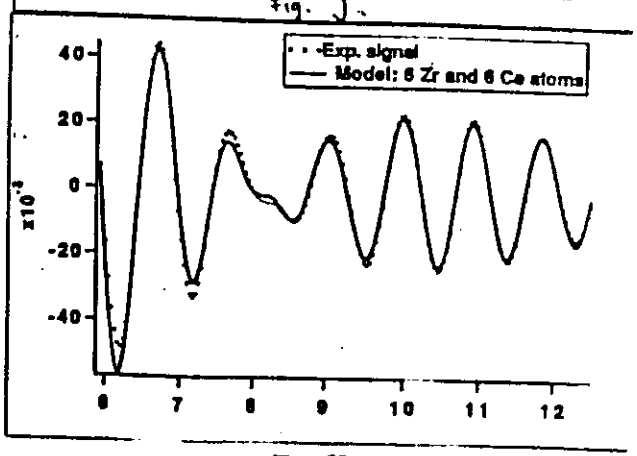

Fig K.

Pic. 12

Pic. 13

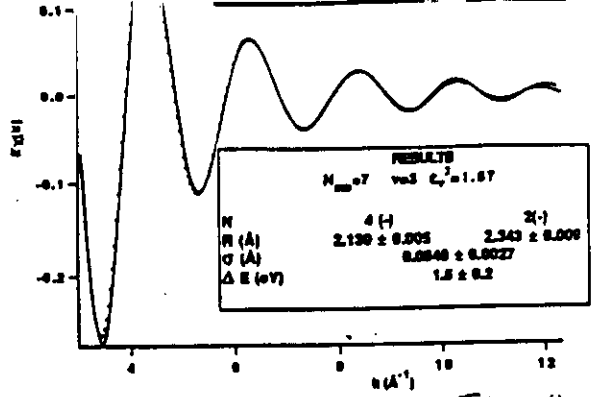

Fig. 16

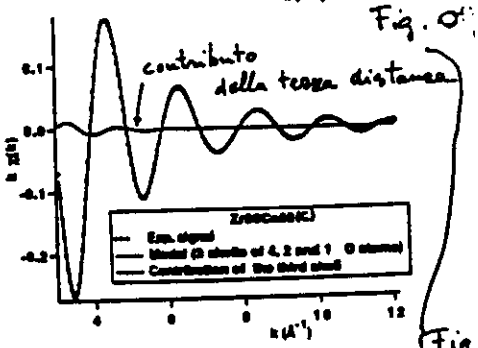

Fig. O

Fig. P

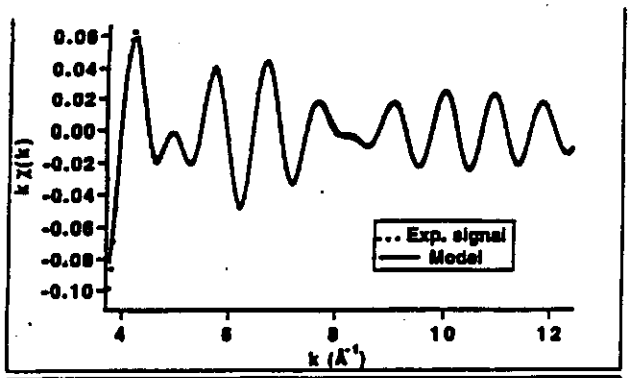

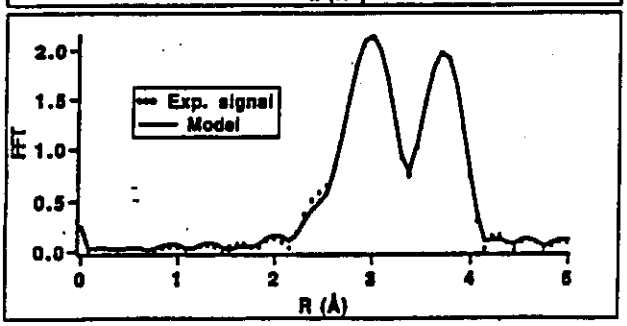

Results of the fit

	N_{IND}=10	v=1	ε_v^2=1.03	
Atom	N	R	σ (Å)	ΔE (eV)
Zr	6(-)	3.64±0.01	0.1057±0.0034	-9.9±4
Ce	6(-)	3.733±0.006	0.0945±0.0035	-6.4±0.6
O	24(-)	4.24±0.03	0.1394±0.0062	-8.1±1.4

Fig. l

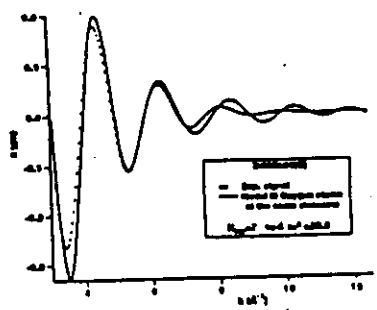

Fig. 15

Fig. m

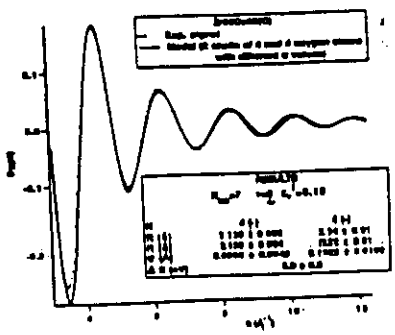

Fig. n